mCardiacDx: Radar-Driven Contactless Monitoring and Diagnosis of Arrhythmia

Arjun Kumar[1], Noppanat Wadlom[1], Jaeheon Kwak[2], Si-Hyuck Kang[3], Insik Shin[1]

***Abstract*—Arrhythmia is a common cardiac condition that can precipitate severe complications without timely intervention. While continuous monitoring is essential for timely diagnosis, conventional approaches such as electrocardiogram (ECG) and wearable devices are constrained by their reliance on specialized medical expertise and patient discomfort from their contact nature. Existing contactless monitoring, primarily designed for healthy subjects, face significant challenges when analyzing reflections from arrhythmia patients due to disrupted spatial stability and temporal consistency caused by underlying irregular heart contractions. In this paper, we introduce mCardiacDx, a radar-driven contactless system that accurately analyzes these complex reflections and reconstructs heart pulse waveforms (HPWs) for arrhythmia monitoring and diagnosis. The key technical contributions of our work include a novel precise target localization (PTL) technique that accurately locates heart reflections despite spatial disruptions, an encoder-decoder model (HPR-Net) that effectively transforms these reflections into HPWs, addressing temporal inconsistencies, and a final analysis module for arrhythmia monitoring and diagnosis. Our evaluation on a dataset of 48 subjects (24 healthy, 24 with arrhythmia) in a seated, daily-life setting shows that both mCardiacDx and the PTL technique significantly outperform the state-of-the-art approach in monitoring and diagnosing arrhythmia.**

Objective: To develop a contactless radar-driven system, mCardiacDx, that overcomes reflection disruption challenges in arrhythmia patients to accurately reconstruct interpretable heart pulse waveforms (HPWs) for monitoring and diagnosis. **Methods and procedures:** We introduce a PTL technique to locate heart reflections despite spatial disruptions, and an encoder-decoder model (HPR-Net) to robustly process reflections and reconstruct interpretable HPWs, addressing temporal inconsistencies. The HPWs are then processed by a final analysis module for arrhythmia monitoring and diagnosis. mCardiacDx is validated against a state-of-the-art approach (baseline) on a dataset of 48 subjects (24 healthy, 24 with arrhythmia) in a seated, daily-life setting. This real-world validation confirms the system's robustness and generalizability to daily-life variations in posture and environment. **Results:** mCardiacDx significantly outperforms the baseline in both monitoring and diagnosis. HPW fidelity (Dynamic time warping (DTW) score) for arrhythmia patients improve from 5.92 to 2.92. HR/RR interval median absolute percentage error (MedAPE) reduced (e.g., HR from 9.10 % to 2.94 %; RR interval from 8.42 % to 2.95 %). Our system achieves superior diagnostic performance with 0.93 accuracy, and 0.91 recall (sensitivity), significantly surpassing the baseline's accuracy of 0.85 and recall of 0.75. **Conclusion:** mCardiacDx is a robust, non-contact system for continuous cardiac care, addressing a critical gap in daily-life arrhythmia monitoring and diagnosis. **Clinical impact:** mCardiacDx offers a passive and continuous solution for arrhythmia monitoring and diagnosis that reduces patient discomfort from wearable devices and enabling consistent detection of cardiac events in home or clinical settings. **Clinical and Translational Impact Statement:** mCardiacDx provides a non-contact solution for arrhythmia monitoring and diagnosis, addressing the critical limitation of existing wearable and contactless devices, and demonstrating high potential for passive, continuous integration into daily home cardiac care.

***Keywords*—Contactless arrhythmia monitoring, Contactless arrhythmia diagnosis, Heart pulse waveform**

I. Introduction

Cardiovascular diseases (CVDs) are the leading cause of death worldwide, with an estimated 20.5 million deaths annually [1]–[3]. As one of the most common types of CVDs, arrhythmia is an abnormal heart rate or rhythm [4] that can lead to severe complications such as stroke or sudden cardiac death. These abnormal rates and rhythms often result from asynchronous and irregular heart contractions [5]–[7]. The prevalence of arrhythmia is currently estimated at 2–9 % of the general population and is expected to increase in the coming years [8]. Therefore, regular monitoring and early diagnosis of arrhythmia are critical to mitigate the risk of adverse events and provide a reference for effective clinical care [9], [10].

Given the significance, arrhythmia diagnostic technologies are rapidly advancing, particularly with the integration of artificial intelligence into these tools. Specifically, the standard method for diagnosing arrhythmias in medical practice involves conducting an electrocardiogram (ECG) examination at healthcare facilities like hospitals, which is inadequate for daily monitoring considering the challenges posed by daily commuting and the substantial involvement of medical professionals. To address this demand, ambulatory ECG devices such as Holter monitors [11]–[13] and ECG patches [14], [15] have been developed. However, these require electrodes to be attached to the skin for long durations, which can disrupt daily activities like sleeping or showering. Additionally, the use of electrodes is not suitable for certain patients, such as newborns and those with skin injuries [16], [17]. Smartwatches with single-lead ECG sensors [18] and photoplethysmography (PPG)-based devices [19]–[21] have also emerged. However, the former requires active user contact to the electrode button, limiting its use for truly continuous monitoring, while the latter is known to cause user discomfort and has a high rate of non-compliance, with 88 % of users removing them before bedtime [22].

To achieve regular cardiac monitoring with passive and continuous benefit, contactless sensing has emerged as a promising solution that leverages Wi-Fi [23], [24], RFID [25], Ultra-Wideband (UWB) [26], and Millimeter-wave (mmWave) radar [27], [28] to detect thoracic wall vibrations. These works monitor the mechanical activity of the chest wall to measure basic heart rate and its variability, often quanti-

[1]Department of Computer Science, KAIST, Korea
[2]Department of Software, Ajou University, Korea
[3]Dept. Internal Medicine, SNUBH, Korea

fied by the RR interval (the time between two successive heartbeats). Furthermore, recent efforts attempt to reconstruct cardiac waveforms from radar reflections like ECG [29]–[31], seismocardiogram (SCG) [32], and photoplethysmogram (PPG) [33], [34]. Existing contactless methods are based on spatially single, stable, and temporally aligned reflections for cardiac waveform reconstruction in healthy subjects with normal heartbeats (synchronous and regular contractions). However, these underlying assumptions fail in arrhythmia patients, where abnormal heartbeats (asynchronous and irregular contractions) create spatially dispersed and temporally misaligned reflections, fundamentally compromising waveform fidelity and diagnostic reliability. For instance, a study on atrial fibrillation (AF) showed that asynchronous and irregular heart contractions produce invalid ECGs without clear cardiac features, preventing arrhythmia diagnosis [35]. The same author in [36] demonstrates successful ECGs reconstruction. However, its reliance on calibration with a traditional ECG patch undermines the claim of being contactless, and its lack of output fidelity makes it unreliable for a true diagnosis. Its performance also declines significantly on unseen patients, indicating poor generalization beyond the training data. Similarly, a recent study [37] introduces a contactless AF monitoring system that achieve clinical-level performance on a large dataset. However, its reliance on a knowledge transfer model ambiguously maps radar features to true cardiac activity, limits interpretability and confidence in the diagnosis. Furthermore, these methods are often limited to controlled, idle postures, restricting their applicability to common daily-life scenarios, such as sitting, where body motion is unavoidable. As noted in [38], [39], body posture significantly affects ECG signals, with seated positions causing more pronounced distortions, showing that methods for controlled postures cannot generalize to daily life scenarios. To sum up, a truly contactless system for monitoring and diagnosing arrhythmia in daily life does not yet exist.

To bridge this gap, we propose mCardiacDx, a radar-driven contactless heart pulse waveforms (HPWs) measurement system that enables passive and continuous arrhythmia monitoring and diagnosis for both healthy and cardiac patients in their daily lives. Fig. 1 illustrates the usage scenarios of mCardiacDx, where we set up a low-cost mmWave radar [8] to sense the subject's thorax wall vibration. We then introduce a custom-designed a signal processing technique and encoder-decoder model to precisely detect heart variations and transfer them into HPWs. The system then employs its heart health analysis module to perform arrhythmia monitoring and diagnosis based on these HPWs. In this way, mCardiacDx can provide an accurate HPWs even during diseases like atrial fibrillation, tachycardia, bradycardia, etc., so as to offer early warnings and better treatment management, specifically through accurate HR and RR interval estimation. To realize mCardiacDx, we identify and address two main challenges as follows.

C1: Locating spatially dispersed and variable-magnitude reflections.

Different from previous works that focused on healthy subjects with synchronous and regular heart contraction,

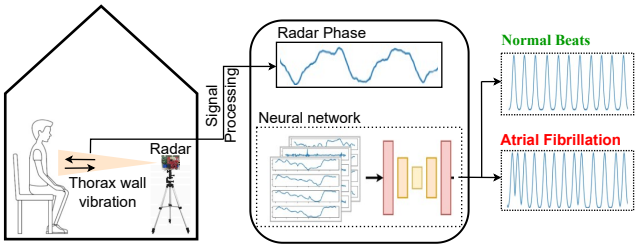

Fig. 1. The usage scenarios of mCardiacDx. mCardiacDx can provide contactless heart pulse waveform for monitoring and diagnosing arrhythmia.

mCardiacDx focuses on reconstructing HPWs during asynchronous and irregular contraction. For healthy subjects, the synchronous and regular heart contraction generates a unified mechanical force on the chest wall, which produces a coordinated and uniform chest-wall vibration, leading to reflections concentrated at a single stable location with consistent magnitude in signal space [40]. However, for arrhythmia patients, asynchronous and irregular contractions generate a scattered mechanical force. In particular, asynchronous and irregular contractions cause the heart chambers (atria and ventricles) to contract at varying times and force, which prevents the force from unifying, thus transferring as multiple, scattered impulses/forces to the chest wall. We infer that this force produces non-uniform chest-wall vibrations, where each vibration acts as a distinct source, resulting in reflections dispersed across multiple unstable locations each exhibiting varying magnitude in signal space [41]. Our statistical analysis across subjects confirms this observation: arrhythmia subjects exhibit a higher mean number of reflection locations (3.8 vs. 1.54) and greater variability in both location count (0.93 vs. 0.64) and reflection magnitude (0.24 vs. 0.05). These findings in arrhythmia patients challenge existing works, which rely on the assumption of a single stable location. This assumption prevents them from locating reflections of varying magnitude dispersed across multiple unstable locations needed for accurate HPW reconstruction. To address this challenge, we introduce a novel precise target localization (PTL) technique, which employs a dynamic processing strategy to locate reflection samples of varying magnitude dispersed across multiple unstable locations for accurate HPW reconstruction.

C2: Interpreting temporally misaligned reflections.

The same underlying physiological factors that cause spatial dispersion and magnitude variation also cause reflections to be temporally misaligned with the underlying ventricular depolarization, which disrupts the predictable pattern of reflections. Healthy subjects exhibit temporally aligned reflections, whereas those from arrhythmia are temporally misaligned. Our statistical analysis between the radar reflections (Phase) and ground truth signal using Zero-Normalized Cross-Correlation (ZNCC) [42] provides quantitative evidence of this degradation, with healthy subjects showing a strong temporal alignment (mean ZNCC of 1.00) while arrhythmia patients exhibit significant misalignment (mean ZNCC of 0.47). The temporal misalignment prevents existing works, which are designed

for temporally aligned reflections, from correctly interpreting such misaligned reflections or distortions for accurate HPW reconstruction. To address this challenge, we propose the heart pulse reconstruction network (HPR-Net), an encoder-decoder model that utilizes graph attention networks (GAT) to interpret the localized multi-bin features derived from PTL and effectively handle their inherent temporal misalignment for accurate HPW reconstruction.

We prototype the end-to-end *mCardiacDx* using texas instruments (TI) AWR1642BOOST mmWave radar [43]. We evaluate mCardiacDx on a dataset of 48 subjects (24 healthy, 24 with arrhythmia) collected during the sitting position in real-world settings in collaboration with a medical professional. We then compare its performance against the state-of-the-art method implemented as a baseline, with all measurements relative to ground truth ECG. Since PTL is a signal processing technique, we examine its performance by integrating PTL into the baseline model, replacing the baseline's conventional technique for locating reflections sources.This serves as component analysis to compare the performance of PTL against a conventional technique. Our results show that both mCardiacDx and the PTL-integrated baseline (baseline+PTL) outperform the baseline in monitoring and diagnosing arrhythmia.

Our results show mCardiacDx and baseline+PTL achieve superior performance in HPW reconstruction, cardiac rhythm monitoring (HR and RR interval), and arrhythmia diagnosis compared to the baseline. For HPW reconstruction, mCardiacDx achieves high fidelity, with dynamic time warping (DTW) [44] scores for arrhythmia patients improving from 5.92 (baseline) to 3.78 (baseline+PTL) and 2.92 (mCardiacDx), indicating accurate waveform alignment during arrhythmia. In HR and RR interval estimation, both methods outperform the baseline, with mCardiacDx achieving the lowest median absolute percentage error (MedAPE) [45] (MedAPE reduced from 9.10 % to 2.94 % for HR and from 8.42 % to 2.95 % for RR interval). For diagnosis, both methods outperform the baseline, with mCardiacDx achieving the best performance, improving recall from 0.75 to 0.91, f1-score from 0.83 to 0.93, and accuracy from 0.85 to 0.93. Results show mCardiacDx is a robust contactless system for pervasive and continuous cardiac care in daily life.

Our contributions can be summarized as follows:

- We propose a novel Precise Target Localization (PTL) technique that can locate the heart reflections dispersed across multiple unstable locations. It addresses the spatial instability caused by asynchronous and irregular contractions in arrhythmia patients, making it possible to reconstruct HPWs.
- We design a novel Heart Pulse Reconstruction Network (HPR-Net) leveraging a Graph Attention Network (GAT) to interpret the temporally misaligned reflections from PTL and transforms them into HPWs that enable monitoring and diagnosis of arrhythmia.
- We prototype and validate the mCardiacDx system on a dataset of 24 patients with various types of arrhythmia in real-world settings. To our knowledge, this is the first contactless system to demonstrate superior monitoring and diagnostic performance through interpretable cardiac waveforms without calibration with any wearables.

II. Understanding Contactless Heart Pulse Waveform

A. Radar Driven Cardiac Sensing

The human heart consists of four chambers—the left atrium (LA), right atrium (RA), left ventricle (LV), and right ventricle (RV)—that work together to manage blood circulation through synchronous and regular contraction. The atria receive blood and pump it into the ventricles, which then store and propel blood throughout the body. The mechanical activity of the heart is generated under the stimulation of electrical activity, where mechanical contraction is initiated by electrical depolarization [46]. This activity is regulated by the heart's electrical conduction system, which initiates at the sinoatrial (SA) node and propagates through the atrioventricular (AV) node, right bundle branch (RBB), left bundle branch (LBB) and the His–Purkinje fibers (PF) network. In healthy subjects, the atria and ventricles contract and relax in synchronous and regular manner due to normal electrical pathways as shown in left side of Fig. 2(b) [47]–[51]. However, this contraction is significantly disrupted in the case of arrhythmia patients due to a chaotic pathways, as shown in right side of Fig. 2(b) [52]–[57].

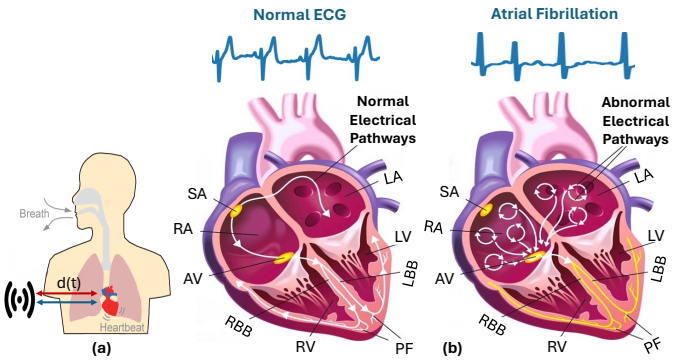

Fig. 2. Contactless Cardiac Sensing and Heart's Morphology with Electrical Pathway. (a) An illustration of radar-based cardiac sensing capturing subtle chest vibrations. (b) A comparison of the electrical pathways in a healthy heart (left) and a heart with arrhythmia (right).

As illustrated in Fig. 2(a), radar-based cardiac sensing captures subtle vibrations on the chest wall during each heartbeat, which are a direct result of the heart's contraction. The radar transmits mmWaves to the chest and receives the reflections. These reflections are represented by the 2-D channel impulse response (CIR) matrix, with dimensions of fast time and slow time due to their different sampling rates [26], [58]. Fast-time corresponds to the range of the reflecting surface, defining range bins where each bin represents a specific spatial location on the chest. Slow-time consists of fast-time snapshots of the reflections (or reflection samples). These samples are taken at a much lower rate, capturing their temporal evolution over

repeated transmissions. Existing works analyzes these reflection samples across both dimensions to extract the chest wall vibration, which is then transformed into cardiac waveforms.

We define the chest wall vibration at time t as $d(t)$, which can be extracted from the phase $\phi(t)$ of the reflection samples using Equation 1, where λ is the mmWave wavelength.

$$d(t) \propto \angle \text{CIR}(t) = \frac{\lambda}{4\pi}\phi(t) \tag{1}$$

Existing contactless works rely on the fundamental assumption that a singular, stable source on the chest wall generates the cardiac reflection samples, which subsequently maps to a singular, stable location (a single range bin) in the radar data. This stability is the key principle for accurate signal processing in healthy subjects. As detailed in the next section, arrhythmia contradicts this norm by creating multiple, unstable sources that map to multiple, unstable locations, challenging this foundational assumption.

B. Limitations of Contactless HPW Reconstruction during Arrhythmia

To achieve contactless monitoring and diagnosis of arrhythmia, reconstructing HPWs from mmWave cardiac reflection samples is a straightforward approach. However, we found that such a solution is not feasible due to the limitations of existing methods. In particular, we implement a state-of-the-art contactless method [32] as a baseline for reconstructing HPWs from mmWave radar reflection samples. In this context, the QRS waveform, particularly R peaks of the ECG correspond to ventricular depolarization, whereas the pulse peaks (P, P') of the HPWs represent the mechanical pulse generated by the subsequent mechanical response (ventricular contraction) that follows depolarization. We denote the ECG R peaks as R, the ECG-derived HPW pulse peaks as P, and the reconstructed HPW pulse peaks as P'. Our results show that the baseline performs well for healthy subjects but fails for arrhythmia patients (Fig.3). For healthy subjects, the reconstructed HPWs are transient, accurate in number, and closely match the ground-truth HPWs derived from the ECG (ECG-derived HPWs). In this case, the pulse peaks P' align well with both P and R (Fig. 3(a)). However, for arrhythmia patients, the reconstructed HPWs are distorted, reduced in number, and poorly match with the ECG-derived HPWs. Here, the P' fails to align with P and R (Fig. 3(b)). This misalignment leads to significantly higher median absolute percentage errors (MedAPE) of 9.10 % and 8.42 % for heart rate (HR) and RR intervals (time between two successive heartbeats, measured between consecutive R and analogously between P and P') in arrhythmia patients compared to much lower errors of 2.66 % and 2.73 % in healthy subjects, all computed relative to the ECG.

The primary cause of this failure stems from two interconnected challenges that the baseline is not designed to address. First, the uncoordinated and non-uniform movements in arrhythmia patients result in spatially dispersed reflection samples of varying magnitudes. This spatial instability conflicts with the baseline 4D cardiac beamformer which uses a convolutional neural network (CNN)-assisted template

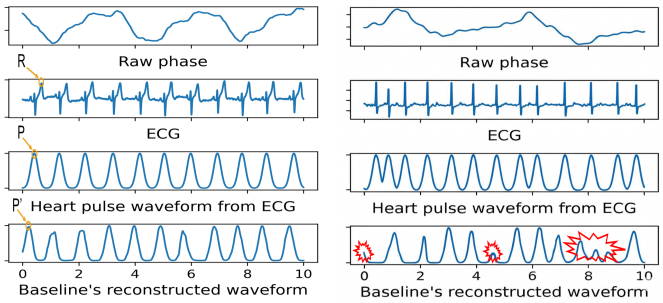

(a) Healthy Subject. (b) Arrhythmia Patient.

Fig. 3. Performance comparison of baseline HPW reconstruction against the ground truth (ECG and ECG-derived HPWs): (a) Successful reconstruction for a healthy subject (b) Reconstruction failure for an arrhythmia patient.

matching to identify the optimal heart reflection sample by assuming a singular, stable source. As a representative case shown in Figure 4, a healthy subject exhibits high-magnitude reflection samples within a single, stable range bin (Fig. 4(a)), whereas an arrhythmia patient shows varying magnitude reflection samples dispersed across multiple unstable range bins (Fig. 4(b)). Our statistical analysis in (I.C1) supported this, which shows greater variability in reflection samples range bin count and magnitude for arrhythmia patients. Without a single, stable location, the baseline beamformer cannot accurately locate cardiac reflection samples in arrhythmia patients. Second, this spatial instability causes temporal misalignment of reflection samples. The baseline translator uses a single-step CNN to learn a static transformation, which assumes a predictable temporal pattern. However, as shown in Figure 3, arrhythmia causes reflection samples to become temporally misaligned with the underlying ventricular depolarization (R-peaks). Cross-correlation analysis between radar and ground-truth signals highlights this, with healthy subjects showing a strong temporal alignment (mean ZNCC of 1.00) (Fig. 5(a)) while arrhythmia patients exhibit significant misalignment (mean ZNCC of 0.47) (Fig. 5(b)) in (I.C2). The single-step translation model cannot account for these temporal inconsistencies. Consequently, the baseline fails to reconstruct HPWs for arrhythmia patients.

Without handling spatially dispersed locations and temporally misaligned reflection samples, existing methods are bounded to fail. For instance, methods using encoder-decoder [35], knowledge transfer [37], and cross-domain diffusion [36] models fail to process the complex, multi-source reflection samples characteristic of arrhythmia.

To address these challenges, we propose a PTL technique to locate reflection samples of varying magnitude dispersed across on multiple stable range bins. We then developed an HPR-Network model with GAT to interpret these reflection samples to reconstruct the HPWs for arrhythmia monitoring and diagnosis.

III. System Overview

In this section, we provide an overview of *mCardiacDx*, a novel, radar-driven contactless system. *mCardiacDx* focuses

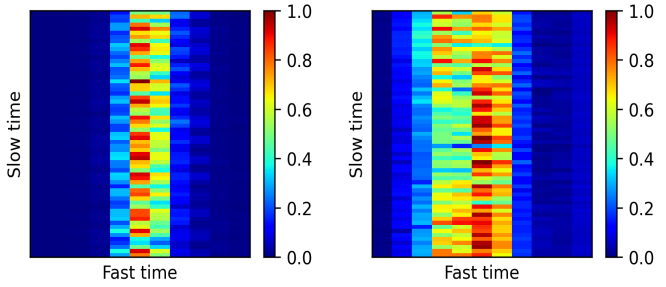

(a) Healthy Subject. (b) Arrhythmia Patient.

Fig. 4. Heart reflection patterns in CIR matrix Illustrating spatial instability. (a) Healthy subjects reflection samples are concentrated into a single, stable range bin exhibiting mostly high magnitude. (b) Arrhythmia patients reflection samples are spatially dispersed across multiple unstable range bins exhibiting varying magnitude.

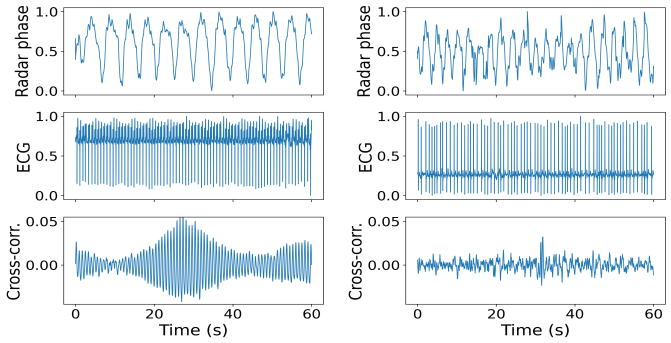

(a) Healthy Subject. (b) Arrhythmia Patient.

Fig. 5. Temporal alignment of heart reflection samples and ECG. (a) Healthy subjects reflections are temporally aligned with ECG, resulting in a strong cross-correlation. (b) Arrhythmia patients reflections are temporally misaligned with the ECG, resulting in weak cross-correlation.

on contactless Heart Pulse Waveform (HPW) reconstruction for monitoring and diagnosis of arrhythmia using mmWave radar reflection samples. Fig. 6 illustrates the architecture of *mCardiacDx*, which mainly consists of four key components to function seamlessly.

mCardiacDx captures the subtle mechanical activities of the heart from the radar reflections, processes them to overcome inherent signal challenges, and subsequently reconstructs high-fidelity HPWs for comprehensive heart health analysis. The core challenges of spatial dispersion and temporal misalignment of reflections are explicitly addressed by our system. Specifically, the workflow of *mCardiacDx* initiates with capture of raw reflection samples from the thorax wall. The system addresses the spatial challenge by employing Precise Target Localization (PTL), which localizes reflection samples dispersed across multiple unstable locations. The output is then refined by Signal Processing to accurately extract the chest wall vibration. Finally, the system leverages the Heart Pulse Reconstruction Network (HPR-Net.) to mitigate the temporal misalignment and synthesize the HPWs, enabling subsequent heart health analysis for monitoring and diagnosis.

The key components of *mCardiacDx* are:

- **Data Acquisition:** The mmWave radar first captures raw reflection samples from the thorax.
- **Precise Target Localization (PTL):** An advanced signal processing technique designed for localization and selection of varying magnitude reflection samples from spatially dispersed locations (range bins), employing a dynamic processing strategy to mitigate spatial dispersion (C1).
- **Signal Processing:** Extracts cardiac motion information from PTL's selected reflection samples, utilizing bandpass and second-order derivative filters to suppress interference and emphasize cardiac motion. **Heart Pulse Reconstruction Network (HPR-Net.):** A deep learning network that leverages the extracted cardiac motion to reconstruct HPWs as Gaussian pulse trains, effectively overcoming temporal misalignment (C2).
- **Heart Health Analysis:** Facilitates comprehensive diagnostics by monitoring HR and RR intervals based on the HPWs, and diagnosing arrhythmia utilizing HR, RR intervals, and various heart rate variability (HRV) metrics.

IV. System Design

In this section, we introduce the detailed technical design of mCardiacDx. We begin with the innovative precise target localization (PTL) technique (Sec. IV-A) used to locate and isolate reflections despite spatial dispersion, followed by the signal processing methods for extracting chest vibration (Sec. IV-B). We then detail the heart pulse reconstruction network (HPR-Net.), which reconstructs HPWs (Sec. IV-C), and conclude with mCardiacDx's heart health analysis module, which performs monitoring and diagnosis (Sec. IV-D).

A. Precise Target Localization

Accurate localization of varying magnitude reflection samples from dispersed across multiple unstable range bins is crucial for accurate HPW reconstruction. The PTL algorithm operates through a sequential two-step process, as detailed in Algorithm 1. In the initial step, the algorithm identifies the target range bin corresponding to the highest magnitude reflection samples. It does this by detecting the high magnitude samples across chirps using the Most Common Bin (MCB) algorithm [32], [59] (lines 1-2). This process enables PTL to locate high magnitude reflection samples consistently concentrated in a single stable range bin. However, this initial step is inadequate for precisely locating reflection samples of varying magnitudes dispersed across multiple unstable range bins, as such samples may dynamically shift between different range bins over time.

To address this limitation, PTL enhances the target selection by implementing a dynamic processing strategy in the second step. It first defines a neighboring window around the target range bin t by computing the first and last bins based on a predefined window breadth w_b (line 3). The w_b is a parameter that determines how many adjacent range bins are considered. This step extracts a sub-matrix that includes surrounding range bins (line 4), enabling the algorithm to capture reflection samples of varying magnitude that dynamically shift across

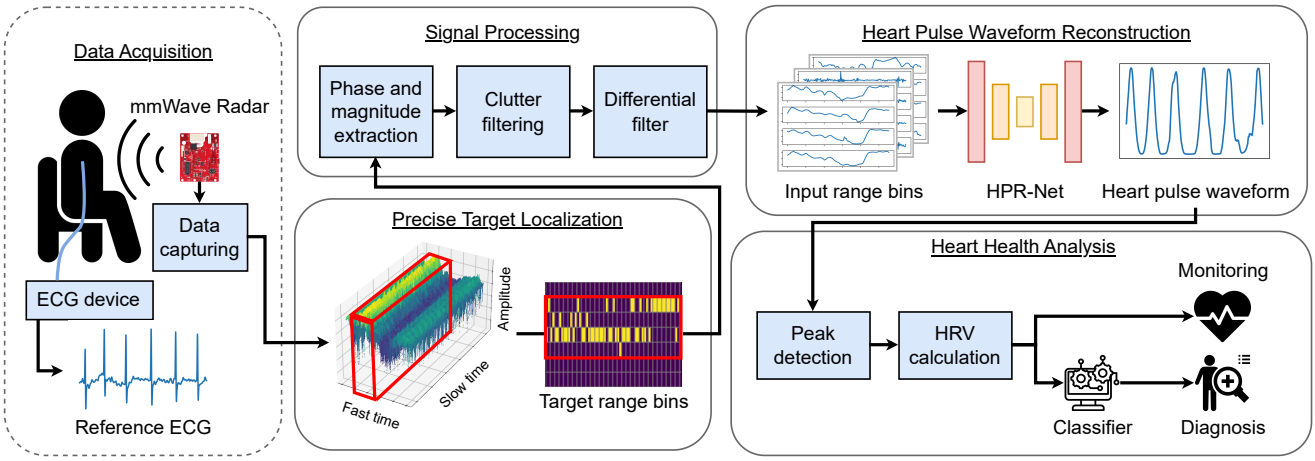

Fig. 6. Schematic overview of mCardiacDx, which captures heart activities through mmWave radar and then transform them into HPWs through PTL and HPR-Network for heart health analysis.

neighboring range bins over time, thereby addressing the limitation of the initial step.

However, merely expanding the range bin selection does not fully account for the dynamic spatial shifts of these reflection samples over time. As these shifts can evolve, it is crucial to continually monitor and track them for precise localization. To address this, PTL iteratively processes chirps within a sliding time window (line 7), extracts data for the current window (line 8), reapplies the MCB algorithm to refine the target range bin t (line 9), and tracks these spatial variations in the identified range bin over time (lines 9–10). This iterative adjustment allows PTL to successfully locate reflection samples with varying magnitude dispersed across multiple unstable range bins. PTL's continual tracking of these spatial variations over time provides a localized and dynamically tracked stream of reflection samples for the subsequent processing stages.

Algorithm 1 PTL Algorithm

Require: CIR matrix $R \in \mathbb{C}^{\text{num\_samples} \times \text{num\_chirps}}$,
Time window size (in number of chirps) $w_t \in \mathbb{Z}$,
Range bin window size $w_b \in \mathbb{Z}$
Ensure: Selected range bins at each chirp $s \in [1, \text{num\_samples}]^{\text{num\_chirps}}$

1: $M \leftarrow \text{abs}(R)$
2: $t \leftarrow \text{MostCommonBin}(M)$
3: first_bin $\leftarrow t - \lfloor \frac{w_b}{2} \rfloor$, last_bin $\leftarrow t + \lceil \frac{w_b}{2} \rceil - 1$
4: $M \leftarrow M[\text{first\_bin} : \text{last\_bin}, :]$
5: $i \leftarrow 1$
6: $s \leftarrow \mathbf{0}^{\text{num\_chirps}}$
7: **while** $i \leq$ num_chirps **do**
8: $M' \leftarrow M[:, i : i + w_t - 1]$
9: $s_{i:i+w_t-1} \leftarrow \text{first\_bin} + \text{MostCommonBin}(M')$
10: $i \leftarrow i + w_t$
11: **end while**

B. Signal Processing

This component transforms the reflection samples selected by PTL into cardiac motion features suitable for HPW reconstruction. We first extract the phase and magnitude signals from the reflection samples, which represent the underlying chest wall vibration, respectively. However, these initial signals contain various physiological motions, including respiration, heartbeat, and other body motions. To isolate the relevant cardiac motion, we apply a bandpass filter (0.2–50 Hz) as a clutter filter. This removes low-frequency baseline drift and high-frequency noise, retaining respiration and cardiac motions. While this filters out general noise, isolating cardiac motion from respiration remains critical. Chest wall vibration caused by respiration is slow with low acceleration, whereas cardiac activity, such as heartbeats, induces significant acceleration. We leverage this fundamental difference in acceleration to distinguish cardiac motion. Therefore, we compute the chest acceleration as the second-order derivative [60] of the chest vibration, which serves as a refined cardiac motion feature that selectively enhances the rapid, high-acceleration components indicative of heartbeats. This filter is defined by equation 2, where ϕ_t represents the phase at time t, and h denotes the sampling interval. Finally, this component provides three distinct processed output, the bandpass-filtered phase and magnitude, and the second-order derivative-filtered phase—for the subsequent HPR-Net.

$$\phi_t'' = \frac{(\phi_{t-3} + \phi_{t+3}) + 2(\phi_{t-2} + \phi_{t+2}) - (\phi_{t-1} + \phi_{t+1}) - 4\phi_t}{16h^2} \tag{2}$$

C. Heart Pulse Reconstruction Network (HPR-Net)

HPR-Net reconstructs HPWs as a series of Gaussian pulse trains. Its end-to-end neural network utilizes phase, the second-order derivative of phase, and magnitude as inputs to extract cardiac motion features for reconstructing HPWs, as shown in Figure 7. Unlike the baseline that interprets features from

temporally aligned reflection samples concentrated to a single stable range bin, HPR-Net is designed to interpret features from the localized multi-bin stream provided by the PTL algorithm (1). While PTL provides some stabilization by consistently selecting the strongest localized reflection at each timestep, the resultant stream still exhibits significant temporal misalignment due to arrhythmia.

To intelligently process this multi-bin input, we employ an attention mechanism inspired by graph attention networks (GAT) [61]. The GAT is essential for robust feature extraction amidst the temporal misalignment of the reflection samples (C2). It adaptively weights the contribution of each range bin at every timestep, allowing the network to robustly focus on the true cardiac motion, even when the magnitude of the motion features shifts between the localized bins. This mechanism captures inter-bin correlations at each timestep, enabling the network to learn robust inter-bin cardiac motion features. These features are then transformed by the subsequent encoder-decoder architecture to derive a cardiac motion latent representation that ultimately leads to the construction of HPWs. The architectural framework of HPR-Net comprises three distinct modules: (1) Heart Signal Extractor, (2) Encoder-Decoder, and (3) Reconstructor, as depicted in Figure 9. Below are detailed descriptions of each module.

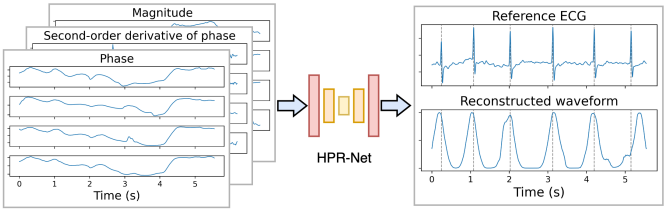

Fig. 7. Example input and output of heart pulse reconstruction network (HPR-Net).

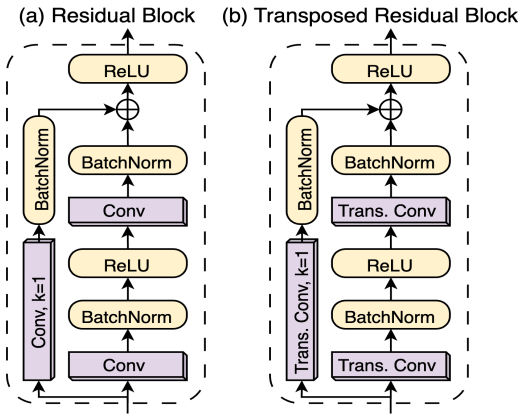

Fig. 8. HPR-Net building blocks: (a) residual block and (b) transposed residual block.

(1) Heart Signal Extractor: This module is designed to extract inter-bin cardiac motion features from the inputs. We begin employing one-dimensional convolutional operations to capture the temporal information within each range bin. To refine the extraction process, we utilize a variant of residual blocks, as depicted in Figure 9. These residual blocks are applied across all range bins selected through PTL, refining the initial features and improving performance and learning efficiency [62].

Subsequently, a GAT mechanism [63] is implemented to model correlations between the range bins. Unlike traditional convolutional networks [64], [65], which assume local spatial correlations, GAT effectively detects relationships between non-adjacent range bins. This capability allows for the accurate detection of patterns within the input features that indicate cardiac motion, thereby facilitating the extraction of relevant inter-bin cardiac motion features. Specifically, at each time step, the GAT block processes a set of temporal features from the range bins, denoted as $\vec{h_i} \in \mathbb{R}^d$ for $i = 1, 2, ..., m$, where d is the dimension of the input features resulting from the convolutional operations and m represents the number of range bins. The learned representation of each range bin's features, $\vec{h_i'} \in \mathbb{R}^{d'}$, where d' is the length of the output features, is computed as:

$$\vec{h_i'} = \sigma\left(\sum_{j=1}^{m} \alpha_{ij} \boldsymbol{W} \vec{h_j}\right) \tag{3}$$

Here, $\boldsymbol{W} \in \mathbb{R}^{d' \times d}$ is a learnable weight matrix, and $\sigma(\cdot)$ denotes the activation function. We employ the Leaky ReLU function with a negative slope of 0.2 as the activation function. The attention coefficient α_{ij} of $\vec{h_j}$ with respect to $\vec{h_i}$ is calculated by:

$$\alpha_{ij} = \frac{\exp\left(\text{LeakyReLU}\left(\vec{a}^T \left[\boldsymbol{W}\vec{h_i} || \boldsymbol{W}\vec{h_j}\right]\right)\right)}{\sum_{k=1}^{m} \exp\left(\text{LeakyReLU}\left(\vec{a}^T \left[\boldsymbol{W}\vec{h_i} || \boldsymbol{W}\vec{h_k}\right]\right)\right)} \tag{4}$$

where $\vec{a} \in \mathbb{R}^{2d'}$ is a learnable weight vector, $[\cdot||\cdot]$ denotes vector concatenation, and LeakyReLU$(\cdot)$ specifies the element-wise Leaky ReLU function with a negative slope of 0.2. The GAT block outputs the inter-bin cardiac motion features within these range bin representations, which are then used by the encoder.

(2) Encoder-Decoder: The encoder module employs a convolutional encoder-decoder (CED) network to construct a cardiac motion latent representation from the extracted inter-bin cardiac motion features. CED networks are known for their efficacy in time series analysis, anomaly detection, and the compression and reconstruction of physiological data, such as ECG [66]–[68]. These networks learn an efficient latent representation of data by transforming the input into a lower-dimensional latent space and then decoding this compressed representation to recover the original data.

Our approach utilizes a CED network with skip connections to achieve this task. The encoder component of the network employs a stack of residual blocks to capture temporal information from the inter-bin cardiac motion features. These residual blocks facilitate the extraction of pertinent temporal characteristics. In contrast, the decoder component employs transposed residual blocks, as shown in Figure 8, to reconstruct the cardiac motion latent representation from the encoded latent space. This encoder-decoder design is essential because

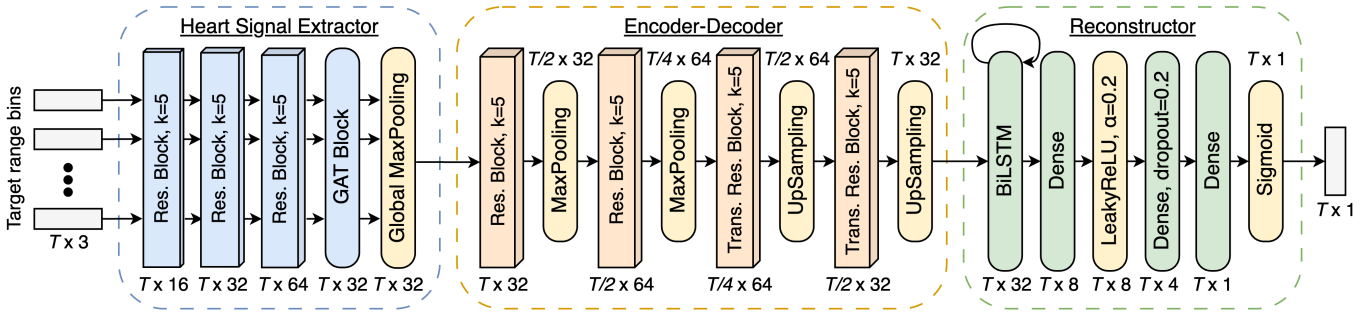

Fig. 9. Architectural overview of the proposed Heart Pulse Reconstruction Network (HPR-Net). The kernel size of each residual block is denoted by k, and each layer is annotated with the shape of its output.

it learns a non-linear transformation that interprets the temporally inconsistent features provided by the GAT and maps them to a smooth, high-level latent representation that restores the underlying temporal order of the cardiac motion. This enables the effective formation of a high-level cardiac motion latent representation.

(3) Reconstructor: The reconstructor module employs a bidirectional long short-term memory (BiLSTM) network to generate the reconstructed HPW from the cardiac motion latent representation. Long short-term memory (LSTM) networks are well-suited for modeling long-range dependencies in time series data, and their bidirectional variant (BiLSTM) further enhances performance by processing the input sequence in both forward and backward directions [69], [70].

In our approach, the cardiac motion latent representation produced by the encoder-decoder module at each time step is fed into the BiLSTM network, as depicted in Figure 9. The BiLSTM captures temporal dependencies and provides a comprehensive understanding of the cardiac motion dynamics, capturing both short-term and long-term relationships in cardiac motion. Following this, a series of dense layers and a sigmoid activation function are applied to compute the amplitude of the cardiac motion waveform at each time step, thereby generating the reconstructed waveform (HPWs).

D. Heart Health Analysis

This component performs both continuous monitoring and arrhythmia diagnosis based on the reconstructed HPWs.

For monitoring, we use a peak detection algorithm [71] to identify the peaks of the HPWs to estimate HR and RR intervals.

The arrhythmia diagnosis model utilizes heart rate variability (HRV) metrics derived from the RR intervals as its input feature set. HRV analysis serves as an effective indicator of cardiac autonomic function; studies often link changes in these metrics to cardiac arrhythmias [72] and autonomic stress responses [73]. Our feature set focuses on six widely accepted time-domain HRV metrics, formally defined based on the RR interval series (NN intervals) [71], [74], [75]: mean of RR intervals (MeanNN), median of RR intervals (MedianNN), standard deviation of RR intervals (SDNN), interquartile range of RR intervals (IQRNN), median absolute deviation of RR intervals (MadNN), and the ratio of MadNN to MedianNN. These metrics are extracted from both the ground-truth ECG readings and the reconstructed HPWs.

For diagnosis, we employ a random forest classifier [76], [77] as our arrhythmia prediction model. This classifier takes the HRV metrics defined above, derived from both the actual ECG readings and the reconstructed HPWs, as its input feature set to diagnose arrhythmias. This approach enables the classifier to utilize information on cardiac variability from both real cardiac activity (ECG) and simulated contactless activity (HPWs), enhancing its ability to differentiate between healthy and arrhythmic conditions. We detail the training and performance of this diagnostic model in Sections V and VI.

V. Implementation and Experimental Details

Hardware and Software Toolkits: We used a texas instruments millimeter wave board (AWR1642BOOST) with the DCA1000 real-time data-capture adapter for precise radar sensing [43], [78]. The board operates in the 77–81 GHz range. We configured the system with 1 transmitter (1Tx) and 4 receivers (4Rx) to enhance spatial resolution while maintaining high temporal resolution through a short chirp period (50 µs) and a high sampling rate (6000 ksps). Each chirp was followed by an idle time of 150 µs, with 256 samples captured per chirp. The receive gain was set to 30 dB, and data acquisition was managed through mmWave Studio [79], which streamed the data to a host PC for processing. Simultaneously, we recorded ECG signals using the shimmer 3TM ECG development kit [80] at a sampling rate of 500 Hz. Radar signal processing was implemented using C/C++, while neural network components were developed in python with tensorflow 2.10 [81] on a workstation with an Intel i7 CPU, 32GB DDR4 RAM, and a NVIDIA GeForce RTX 2070 graphics card [82].

Participant: We collected data from 210 participants (ages 32–68), comprising 108 healthy subjects from the general population and 102 patients diagnosed with arrhythmia. Data from healthy subjects was collected at our institution (KAIST), Korea, while data from arrhythmia patients was collected in collaboration with a renowned cardiologist from Seoul National University Bundang Hospital, Korea. The study was conducted under university Institutional Review Board

(a) Setup at KAIST.

(b) Setup at SNU Hospital.

Fig. 10. Experimental setups for data collection. (a) Setup at KAIST. (b) Setup at SNU Hospital.

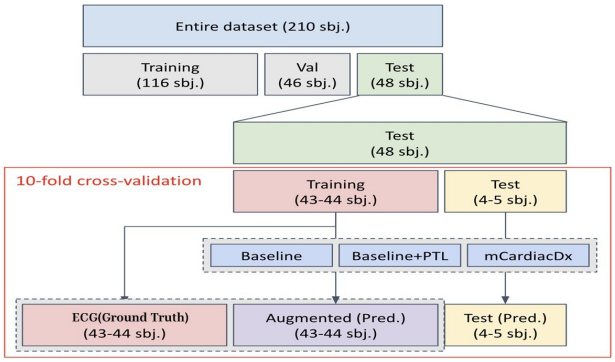

Fig. 11. Overview of the dataset split for diagnosis model training and testing.

(IRB) approval, ensuring adherence to ethical guidelines. All participants were briefed on the study objectives, provided written consent before participation, and were compensated for their time. They were also instructed to minimize voluntary movement during recording sessions to ensure consistent data acquisition.

Data Collection Procedure: The data collection process involved the simultaneous acquisition of radar and ECG recordings from each participant. This was conducted in a typical office environment that included standard furniture and ambient wireless signals such as WiFi, LTE, and Bluetooth, simulating real-life conditions. During data collection, the radar was positioned to capture reflections directly from the participant's chest, as shown in Figure 10. At the same time, ECG data was collected using the shimmer ECG, with electrodes placed on four locations: the left arm (LA), right arm (RA), left leg (LL), and right leg (RL). Both healthy participants and arrhythmia patients were seated 25 to 55 cm away from the radar. Participants were instructed to breathe normally and minimize voluntary movements to ensure consistent readings.

A total of 210 trials were conducted, each lasting 60 seconds, resulting in a dataset of approximately 20,000 heartbeats. The recorded heart rates ranged from 67 to 97 beats per minute (bpm) for healthy subjects and from 55 to 115 bpm for arrhythmia patients. To ensure the robust performance of the baseline, baseline+PTL, and mCardiacDx systems in reconstructing HPWs and to diagnose arrhythmia, we randomly partitioned the dataset into training, validation, and test sets, following a 60/24/24 split for healthy subjects and 56/22/24 for arrhythmia patients.

Network and Model Training: We detail the network and model training below:

- *HPR-Net Training:* The neural networks for the baseline, baseline+PTL, and mCardiacDx for HPW reconstruction were trained on the training set for 300 epochs using an Adam optimizer. For the baseline and baseline+PTL models, training was performed using a batch size of 16 and an initial learning rate of 0.001. Similarly, the mCardiacDx model was trained using a batch size of 16 and an initial learning rate of 0.0005.
- *Diagnosis:* The random forest model was trained on a combined feature set of HRV metrics. This set included metrics derived from ground truth ECG. These ECG-derived metrics were augmented by additional similar HRV metrics derived from the HPWs generated by the three systems (baseline, baseline+PTL, and mCardiacDx), as illustrated in Figure 11. This approach enables the model to learn directly from both original and system-augmented metrics, which enhance its foundation for robust arrhythmia diagnosis. For testing, model extracts similar metrics derived from the HPWs of the corresponding system.

VI. Performance Results

In this section, we evaluate the performance of baseline+PTL and mCardiacDx in comparison to the baseline using the evaluation metrics outlined in section VI-A. Our analysis focuses on both healthy subjects and arrhythmia patients, emphasizing three main areas: the quality of HPWs reconstruction, the monitoring of HR and RR intervals, and the diagnosis of arrhythmias.

A. Evaluation Metrics

We employed the following set of quantitative metrics [44], [45], [83] for each evaluation stage:

1) HPW Reconstruction Quality:

- *Dynamic Time Warping (DTW):* DTW [44] measures the similarity between two-time series that may vary in speed or timing. For HPW reconstruction, we use DTW to quantify the similarity between systems HPWs and ECG-generated HPWs. Lower DTW scores indicate higher similarity and better reconstruction.

2) Heart Rate(HR) and RR Interval Estimation Accuracy:

- *Median Absolute Percentage Error (MedAPE):* MedAPE [45] quantifies the median absolute percentage difference between estimated values (HR and RR intervals from systems) and ECG. Lower MedAPE values signify higher estimation accuracy.

3) Arrhythmia Diagnosis Performance: For evaluating the diagnostic capabilities, we use standard binary classification metrics [83] derived from the confusion matrix, where the arrhythmia is considered the positive class and healthy is the negative class:

- *Accuracy:* Proportion of all correctly classified instances, defined as $\text{Accuracy} = (\text{TP}+\text{TN})/(\text{TP}+\text{FN}+\text{FP}+\text{TN})$.
- *Precision:* Proportion of true positive predictions among all predictions. It measures the model's ability to avoid false positives, defined as $\text{Precision} = \text{TP}/(\text{TP}+\text{FP})$.
- *Recall (Sensitivity):* Proportion of true positive predictions among all actual positive instances. It measures the model's ability to identify all relevant cases, avoiding false negatives, defined as $\text{Recall} = \text{TP}/(\text{TP}+\text{FN})$.
- *F1-score:* The harmonic mean of precision and recall, balancing both. It is a key metric in arrhythmia diagnosis, calculated as $\text{F1-score} = 2\times(\text{Precision}\times\text{Recall})/(\text{Precision}+\text{Recall})$.
- *Receiver Operating Characteristic (ROC):* Measures the ability of a classifier to distinguish classes across various threshold settings. A ROC value of 1.0 represents a perfect classifier, while 0.5 indicates a random chance.

B. Reconstructing the Heart Pulse Waveform

e evaluate the performance of our proposed methods, baseline+PTL and the mCardiacDx system, in reconstructing heart pulse waveforms (HPWs) and compare them against the baseline. The primary goal is to evaluate their ability to overcome the baseline's previously identified failure in reconstructing HPWs, which, as shown, leads to significant errors in HR and RR interval estimation. A qualitative analysis, shown in Figure 12, illustrates the performance of each method. For healthy subjects, all three approaches successfully reconstruct HPWs that align well with the ECG-derived HPWs (Figure 12(a)). However, a critical distinction appears in arrhythmia cases. As established previously, the baseline method produces distorted HPWs, reduced in number and poorly aligned with the ECG-derived HPWs (as highlighted in red). As shown in Figure 12(b), both baseline+PTL and mCardiacDx successfully reconstruct the HPWs for arrhythmia patients. Notably, mCardiacDx achieves the highest fidelity, generating the correct number of HPWs and exhibiting the closest alignment to the ECG-derived HPWs, surpassing the improvement offered by PTL alone.

To quantitatively validate these findings, we compare the reconstructed HPWs directly with the ECG-derived HPWs. For this, we use dynamic time warping (DTW), a metric ideal for measuring the similarity between time-series data that may have timing variations. A lower DTW score indicates that the reconstructed HPW is more similar to the ECG-derived HPWs. The results shown in Figure 13 confirm the superiority of our methods. For arrhythmia patients, the baseline exhibits a high DTW score of 5.92, reflecting poor performance. The introduction of our PTL technique (baseline+PTL) significantly reduces this score to 3.78. Our complete mCardiacDx system achieved the best score of 2.92, indicating the most accurate waveform reconstruction. This trend also holds for healthy subjects, where mCardiacDx (2.82) and baseline+PTL (3.90) outperform the baseline (4.02). Collectively, these results demonstrate that both PTL and the mCardiacDx system effectively address the baseline's limitations, enabling the

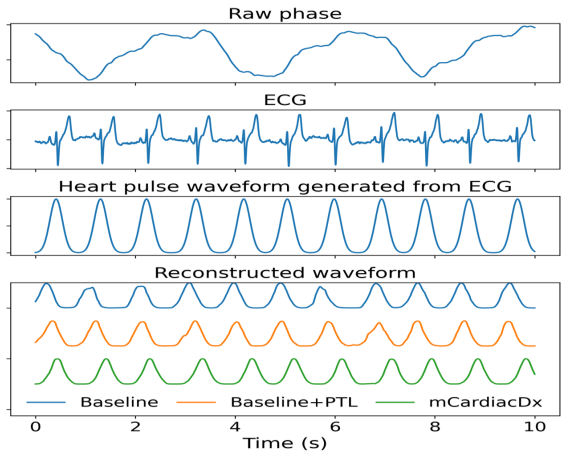

(a) Healthy subjects.

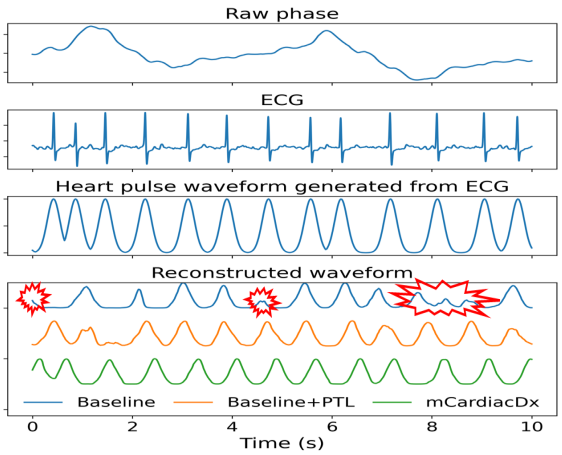

(b) Arrhythmia Patients.

Fig. 12. Performance comparison of baseline, baseline+PTL and mCardiacDx HPW reconstruction against the ECG-derived HPWs

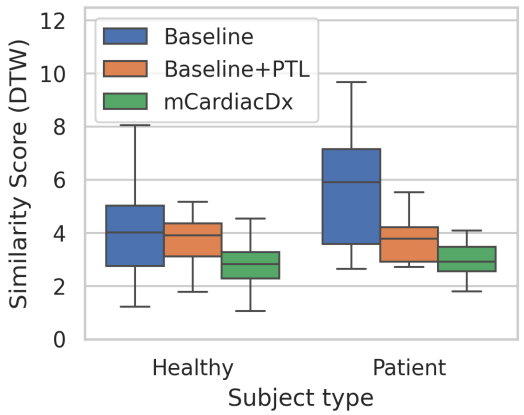

Fig. 13. Dynamic time warping (DTW) scores of mCardiacDx and baseline+PTL compared to the baseline.

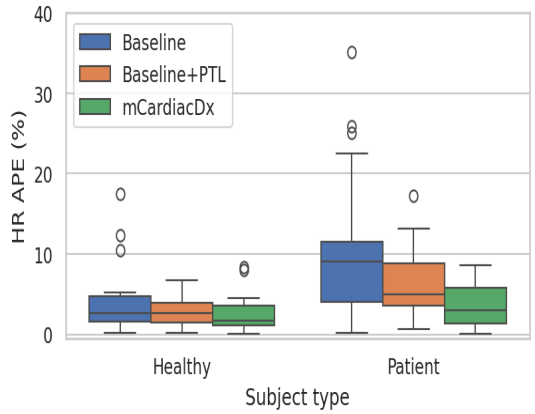

(a) MedAPE of HR.

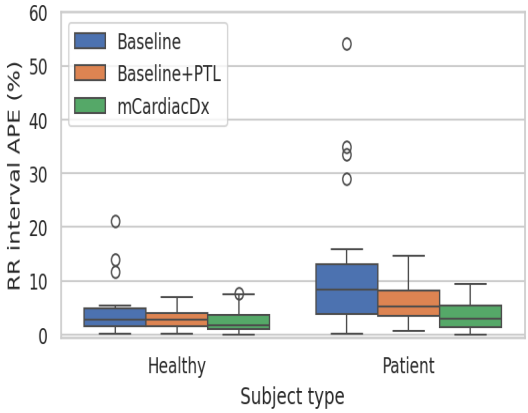

(b) MedAPE of RR Intervals.

Fig. 14. Monitoring Performance of mCardiacDx and baseline+PTL compared to the baseline.

accurate reconstruction of HPWs that faithfully match the ECG-derived HPWs, even in challenging arrhythmia cases.

C. Monitoring Arrhythmia

We evaluate the monitoring performance of baseline+PTL and mCardiacDx in estimating HR and RR intervals based on the reconstructed HPWs. We measure their performance using the MedAPE, calculated relative to ground truth ECG, and compare it against the baseline method. Figure 14 illustrates that both baseline+PTL and mCardiacDx consistently achieve lower MedAPE error rates for HR and RR intervals estimation across both healthy and arrhythmia subject groups. For the healthy group, baseline+PTL achieves error rates of 2. 63% and 2. 70% for HR and RR intervals, showing a reduction compared to baseline errors of 2.66% and 2.73%, respectively. mCardiacDx further reduces these errors to 1.68% and 1.71% for HR and RR intervals. For the arrhythmia group, baseline+PTL yielded error rates of 4.95% and 5.21% for HR and RR intervals, which are significantly lower than the baseline errors of 9.10% and 8.42%. mCardiacDx further reduced these errors to 2.94% and 2.95% for HR and RR intervals. These results strongly indicate that both baseline + PTL and mCardiacDx are robust in monitoring arrhythmias.

D. Diagnosing Arrhythmia

We further evaluate the diagnostic capabilities of baseline+PTL and mCardiacDx, comparing their performance to the baseline approach in diagnosing arrhythmia. The findings are presented in the subsequent subsections.

Baseline: It demonstrates considerable diagnostic performance for healthy subjects, achieving a precision of 0.94 with 1 false positive. However, its recall was limited to 0.7500, resulting in 6 false negatives among the 24 arrhythmia patients, indicating significant challenges in diagnosing arrhythmia cases. While it correctly identifies 23 out of 24 healthy cases and an overall accuracy of 0.8500, the F1-score of 0.83 reflects a moderate balance between precision and recall. The ROC of 0.97 (actual 0.9661) indicates good discriminative ability, though the model's limitations in diagnosing arrhythmia patients prompt further improvements through PTL. The results are illustrated in the confusion matrix and ROC curve plots in Figure 15(a) and (b).

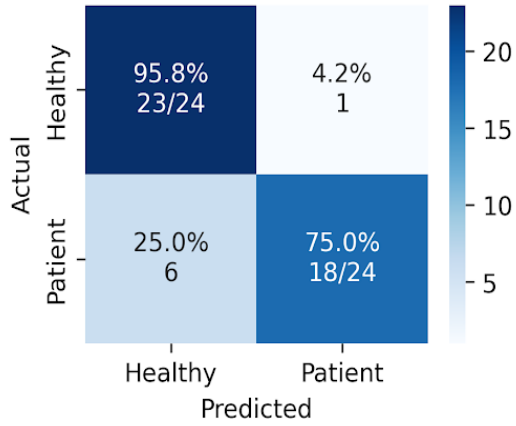

(a) Confusion Matrix.

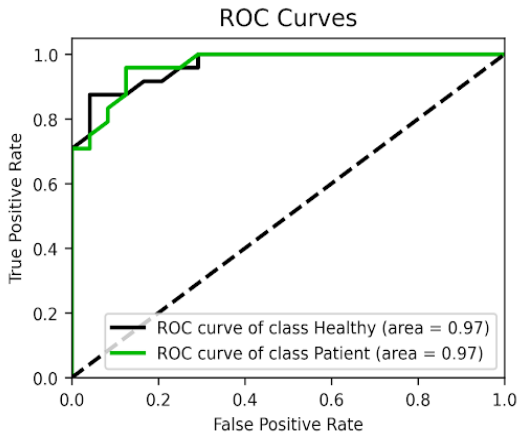

(b) ROC Curves.

Fig. 15. Diagnosis Performance of the baseline.

Baseline+PTL: The baseline+PTL shows improvements over the baseline. Its precision and recall increase to 0.95 and 0.83, respectively, with 1 false positive consistent with the baseline. It diagnoses 20 true positives and reduces false negatives to 4, demonstrating improved sensitivity. While

correctly identifying 23 out of 24 true negatives, it achieves an improved F1-score of 0.88, indicating better balance between precision and recall. The overall accuracy increases to 0.89 and the ROC reaches 0.97 (actual 0.9679), demonstrating strong discriminative capacity. Despite these advancements, the remaining false negatives indicate room for improvement, which is addressed by our system mCardiacDx. Nonetheless, baseline+PTL proves to be a more effective solution for diagnosing arrhythmia compared to the baseline. The results are shown in the confusion matrix and ROC curve plots in Figure 16(a) and (b).

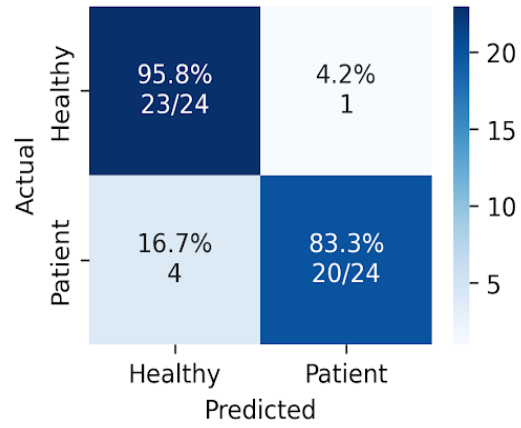

(a) Confusion Matrix.

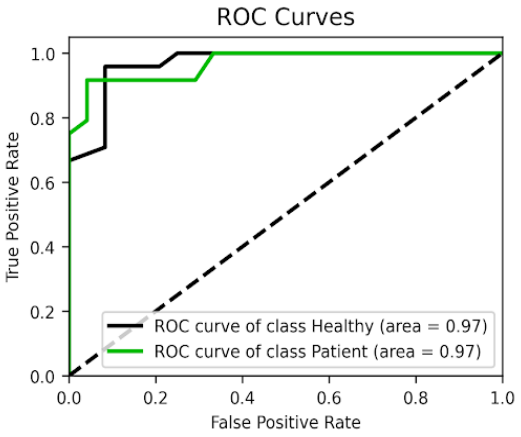

(b) ROC Curves.

Fig. 16. Diagnosis Performance of the baseline+PTL.

mCardiacDx: The mCardiacDx further advances the diagnostic capabilities, achieving a precision of 0.95 with 1 false positive consistent with the baseline. Its recall improves significantly to 0.91, diagnosing 22 true positives with only 2 false negatives, thus outperforming both the baseline and baseline+PTL in sensitivity. While correctly identifying 23 out of 24 true negatives, mCardiacDx demonstrates superior performance with an F1-score of 0.93 and overall accuracy of 0.93. The ROC improves to 0.98, affirming its outstanding discriminative capability. This performance positions mCardiacDx as a leading solution for contactless arrhythmia monitoring. The results are shown in the confusion matrix and ROC curve plots in Figure 17(a) and (b).

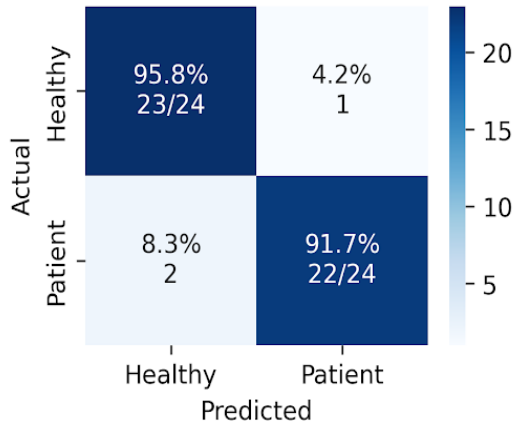

(a) Confusion Matrix.

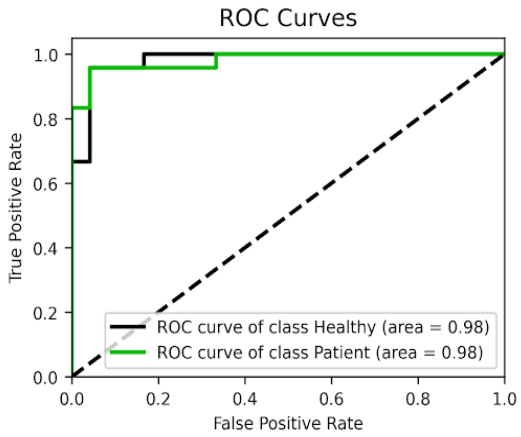

(b) ROC Curves.

Fig. 17. Diagnosis Performance of the mCardiacDx.

VII. Related Work

In this section, we review existing studies on monitoring heart activity, with a particular focus on arrhythmia. We categorize these approaches into two main categories: *wearable cardiac sensing* and *contactless cardiac sensing*.

Wearable cardiac sensing: Wearable cardiac sensing primarily employs two key modalities: electrocardiography (ECG) [9], [13]–[15], [18], [84], [85] and photoplethysmography (PPG) [19]–[21]. ECG has traditionally been regarded as the gold standard for arrhythmia diagnosis in clinical environments such as hospitals [9], [84], [85]. However, its application for continuous monitoring outside these settings has been challenging due to the requirement for medical expertise. To address this challenge, recent advancements have led to the creation of portable ECG devices, including Holter monitors [11]–[13] and ECG patches [14], [15]. While these devices enhance convenience, they require the attachment of electrodes to the skin for longer duration, which can disrupt daily activities like sleeping or showering. Beside, the electrode attachment makes them unsuitable for certain populations, such

as newborns, the elderly, and patients with skin burns. Newly released single-lead ECG sensors integrated into smartwatches provide another option but require active user interaction, specifically touching an electrode button during monitoring, which prevents their use for continuous monitoring [18]. In addition to ECG, PPG-based wearables offer a convenient alternative for arrhythmia detection [19]–[21]. Despite this convenience, long-term use can cause discomfort and skin allergies. A study found that 88 % of users remove their watches before bed [22].

Contactless cardiac sensing: Contactless cardiac sensing has emerged as an alternative to traditional wearable sensing by leveraging radio frequency (RF) signals, such as WiFi [23], [24], RFID [25], ultra-wideband (UWB) [26], and mmWave radar [27], [28], to monitor heart rate (HR) and heart rate variability (HRV). These systems detect thoracic wall vibrations to infer mechanical motions associated with the cardiac cycle. Research has extended contactless sensing to support applications like emotion recognition [28] and stress detection [86]. Notably, advancements have focused on reconstructing cardiac waveforms, such as seismocardiograms (SCG), which reflect mechanical activity of atrial and ventricular contraction. For example, radar systems enhanced with multichannel beamforming and one-dimensional 1-D CNNs have been used to extract SCG features [32]. Recently, research has shifted toward reconstructing electrocardiogram (ECG) waveforms from mmWave reflections using generative models [29]–[31]. CardiacWave [30] introduced an attention-augmented LSTM-based CaSE-ECG solver to recover ECG-like signals, whereas RF-ECG [31] used a conditional generative adversarial network (cGAN) to synthesize ECG waveforms. In parallel, other studies have explored the reconstruction of photoplethysmogram (PPG) waveforms from mmWave signals to infer vascular and respiratory dynamics [33], [34]. However, these studies primarily focused on healthy subjects with normal heartbeats.

More recently, studies have focused on patients with abnormal heartbeats exhibiting asynchronous and irregular heart contractions. Zhao et al. [35] showed that asynchronous heart contractions in atrial fibrillation (AF) create a challenge in cardiac waveform generation. Acknowledging this, the authors proposed a classification-based approach to identify arrhythmia based on radar signal patterns. Although innovative, this method produces a 'black box' output that fails to provide crucial temporal features required for diagnosis. In a related study, the same author focused on reconstructing cardiac waveforms, particularly ECGs, using a cross-domain diffusion model [36]. However, this method requires calibration with a traditional ECG, undermining its fully contactless claim, and the outputs lack necessary fidelity for diagnosis. Its performance declines in unseen patients, indicating limited generalization beyond training data. Similarly, Yuan et al. [37] introduced an AF monitoring system employing a knowledge transfer approach using a teacher-student model pretrained on contact-based ECG data. While innovative, the mapping between radar-based features and true cardiac activity remains ambiguous, limiting contactless feature interpretability and confidence in diagnosis.

Distinct from prior work, *mCardiacDx* and *Baseline+PTL* facilitate the monitoring and diagnosis of arrhythmia by contactless creation of cardiac waveforms in the form of HPWs, which provide the temporal features required for clinical diagnosis—all without relying on calibration with a traditional ECG. More specifically, our system is designed to perform the monitoring and diagnosis of arrhythmia on real patients in practical daily life scenarios, a critical advancement over existing methods.

VIII. Limitations and Future Work

While the proposed **mCardiacDx** system and PTL technique show promise in monitoring and diagnosing arrhythmia, the current implementation is limited to patients in quiescent or minimally-moving states (e.g., seated, as evaluated). This constraint poses a significant challenge for accurately monitoring patients during dynamic motions such as walking on the treadmill, cycling. Moreover, the system currently focuses on reconstructing HPWs, which, although effective, provide limited insight into detailed cardiac dynamics.

Future work will aim to extend the system and technique to support monitoring and diagnosis under motion. This includes developing motion-robust signal processing techniques to manage distortion and variability introduced by movement (walking on the treadmill, cycling, etc). Furthermore, we plan to extend capability of *mCardiacDx* to reconstruct detailed cardiac cycles, enabling analysis comparable to conventional ECG in terms of atrial and ventricular activity. Another important direction involves investigating the relationship between spatially dispersed and temporally misaligned reflections characteristics and arrhythmia severity.

IX. Conclusion

In this paper, we present mCardiacDx, a radar-driven contactless system designed for arrhythmia monitoring and diagnosis. The system leverages a PTL technique to analyze complex reflections and reconstruct HPWs for estimating key cardiac rhythm metrics (HR and RR interval). Evaluation results demonstrate that mCardiacDx, powered by PTL, outperforms state-of-the-art work in monitoring and diagnosing arrhythmia. mCardiacDx is a robust contactless system for pervasive and continuous cardiac care in daily life.

References

[1] World Health Organization, "Cardiovascular diseases (cvds)," 2024. Accessed: 2024-10-29.
[2] World Heart Federation, "Atrial fibrillation infographic," 2024. Accessed: 2024-10-29.
[3] World Heart Federation, "World heart report 2023," 2023. Accessed: 2024-10-29.
[4] Y.-F. Xiao, "Cardiac arrhythmia and heart failure: From bench to bedside," *Journal of Geriatric Cardiology: JGC*, vol. 8, no. 3, p. 131, 2011.
[5] B. Gorenek, C. Blomström Lundqvist, J. Brugada Terradellas, A. J. Camm, G. Hindricks, K. Huber, P. Kirchhof, K.-H. Kuck, G. Kudaiberdieva, T. Lin, *et al.*, "Cardiac arrhythmias in acute coronary syndromes: position paper from the joint ehra, acca, and eapci task force," *EP Europace*, vol. 16, no. 11, pp. 1655–1673, 2014.

[6] T. Higaki, C. Kondo, H. Tomimatsu, E. Yamamura, E. Yamamoto, K. Konishi, M. Nagashima, and T. Nakanishi, "Asynchronous contraction of the 2 ventricles caused by ventricular pacing after a fontan-type operation in a patient with a biventricular heart," *International Journal of Cardiology*, vol. 150, no. 3, pp. e116–e118, 2011.

[7] L. Zhang, B. Li, and L. Wu, "Heart rate variability in patients with atrial fibrillation of sinus rhythm or atrial fibrillation: chaos or merit?," *Annals of medicine*, vol. 57, no. 1, p. 2478474, 2025.

[8] Arrhythmia Alliance, "Arrhythmia facts and statistics: What you need to know," 2025. Accessed: 2025-09-26.

[9] H. Calkins, M. R. Reynolds, P. Spector, M. Sondhi, Y. Xu, A. Martin, C. J. Williams, and I. Sledge, "Treatment of atrial fibrillation with antiarrhythmic drugs or radiofrequency ablation: two systematic literature reviews and meta-analyses," *Circulation: Arrhythmia and Electrophysiology*, vol. 2, no. 4, pp. 349–361, 2009.

[10] J. A. López-López, J. A. Sterne, H. H. Thom, J. P. Higgins, A. D. Hingorani, G. N. Okoli, P. A. Davies, P. N. Bodalia, P. A. Bryden, N. J. Welton, *et al.*, "Oral anticoagulants for prevention of stroke in atrial fibrillation: systematic review, network meta-analysis, and cost effectiveness analysis," *bmj*, vol. 359, p. NA, 2017.

[11] A. Y. Hannun, P. Rajpurkar, M. Haghpanahi, G. H. Tison, C. Bourn, M. P. Turakhia, and A. Y. Ng, "Cardiologist-level arrhythmia detection and classification in ambulatory electrocardiograms using a deep neural network," *Nature medicine*, vol. 25, no. 1, pp. 65–69, 2019.

[12] M. P. Turakhia, D. D. Hoang, P. Zimetbaum, J. D. Miller, V. F. Froelicher, U. N. Kumar, X. Xu, F. Yang, and P. A. Heidenreich, "Diagnostic utility of a novel leadless arrhythmia monitoring device," *The American journal of cardiology*, vol. 112, no. 4, pp. 520–524, 2013.

[13] "Holter monitor." https://en.wikipedia.org/wiki/Holter_monitor, 2025. Accessed: 2025-09-24.

[14] M. Yenikomshian, J. Jarvis, C. Patton, C. Yee, R. Mortimer, H. Birnbaum, and M. Topash, "Cardiac arrhythmia detection outcomes among patients monitored with the zio patch system: a systematic literature review," *Current medical research and opinion*, vol. 35, no. 10, pp. 1659–1670, 2019.

[15] CarePulse, "Carepulse index - home." https://index.carepulse.cn/home/index.html, 2025. Accessed: 2025-09-26.

[16] A. R. Almalty, S. H. Hamed, M. Y. Jebril, and H. M. Abdelnour, "The effect of electrical stimulation on skin vulnerability to irritants," *Skin Research and Technology*, vol. 30, no. 2, p. e13591, 2024.

[17] A. B. Nigusse, D. A. Mengistie, B. Malengier, G. B. Tseghai, and L. V. Langenhove, "Wearable smart textiles for long-term electrocardiography monitoring—a review," *Sensors*, vol. 21, no. 12, p. 4174, 2021.

[18] N. Isakadze and S. S. Martin, "How useful is the smartwatch ecg?," *Trends in cardiovascular medicine*, vol. 30, no. 7, pp. 442–448, 2020.

[19] Y. Guo, H. Wang, H. Zhang, T. Liu, Z. Liang, Y. Xia, L. Yan, Y. Xing, H. Shi, S. Li, *et al.*, "Mobile photoplethysmographic technology to detect atrial fibrillation," *Journal of the American College of Cardiology*, vol. 74, no. 19, pp. 2365–2375, 2019.

[20] M. V. Perez, K. W. Mahaffey, H. Hedlin, J. S. Rumsfeld, A. Garcia, T. Ferris, V. Balasubramanian, A. M. Russo, A. Rajmane, L. Cheung, *et al.*, "Large-scale assessment of a smartwatch to identify atrial fibrillation," *New England Journal of Medicine*, vol. 381, no. 20, pp. 1909–1917, 2019.

[21] H. Zhang, L. Zhu, V. Nathan, J. Kuang, J. Kim, J. A. Gao, and J. Olgin, "Towards early detection and burden estimation of atrial fibrillation in an ambulatory free-living environment," *Proceedings of the ACM on Interactive, Mobile, Wearable and Ubiquitous Technologies*, vol. 5, no. 2, pp. 1–19, 2021.

[22] H. Jeong, H. Kim, R. Kim, U. Lee, and Y. Jeong, "Smartwatch wearing behavior analysis: a longitudinal study," *Proceedings of the ACM on Interactive, Mobile, Wearable and Ubiquitous Technologies*, vol. 1, no. 3, pp. 1–31, 2017.

[23] X. Wang, C. Yang, and S. Mao, "Phasebeat: Exploiting csi phase data for vital sign monitoring with commodity wifi devices," in *2017 IEEE 37th international conference on distributed computing systems (ICDCS)*, pp. 1230–1239, IEEE, 2017.

[24] X. Wang, C. Yang, and S. Mao, "On csi-based vital sign monitoring using commodity wifi," *ACM Transactions on Computing for Healthcare*, vol. 1, no. 3, pp. 1–27, 2020.

[25] J. Ning, L. Xie, C. Wang, Y. Bu, F. Xu, D.-W. Zhou, S. Lu, and B. Ye, "Rf-badge: Vital sign-based authentication via rfid tag array on badges," *IEEE Transactions on Mobile Computing*, vol. 22, no. 2, pp. 1170–1184, 2021.

[26] Z. Chen, T. Zheng, C. Cai, and J. Luo, "Movi-fi: Motion-robust vital signs waveform recovery via deep interpreted rf sensing," in *Proceedings of the 27th annual international conference on mobile computing and networking*, (-), pp. 392–405, ACM, 2021.

[27] F. Wang, X. Zeng, C. Wu, B. Wang, and K. R. Liu, "mmhrv: Contactless heart rate variability monitoring using millimeter-wave radio," *IEEE Internet of Things Journal*, vol. 8, no. 22, pp. 16623–16636, 2021.

[28] M. Zhao, F. Adib, and D. Katabi, "Emotion recognition using wireless signals," in *Proceedings of the 22nd annual international conference on mobile computing and networking*, pp. 95–108, 2016.

[29] J. Chen, D. Zhang, Z. Wu, F. Zhou, Q. Sun, and Y. Chen, "Contactless electrocardiogram monitoring with millimeter wave radar," *IEEE Transactions on Mobile Computing*, vol. 23, no. 1, pp. 270–285, 2022.

[30] C. Xu, H. Li, Z. Li, H. Zhang, A. S. Rathore, X. Chen, K. Wang, M.-c. Huang, and W. Xu, "Cardiacwave: A mmwave-based scheme of non-contact and high-definition heart activity computing," *Proceedings of the ACM on Interactive, Mobile, Wearable and Ubiquitous Technologies*, vol. 5, no. 3, pp. 1–26, 2021.

[31] Z. Wang, B. Jin, S. Li, F. Zhang, and W. Zhang, "Ecg-grained cardiac monitoring using uwb signals," *Proceedings of the ACM on Interactive, Mobile, Wearable and Ubiquitous Technologies*, vol. 6, no. 4, pp. 1–25, 2023.

[32] U. Ha, S. Assana, and F. Adib, "Contactless seismocardiography via deep learning radars," in *Proceedings of the 26th annual international conference on mobile computing and networking*, (London, UK), pp. 1–14, ACM New York, NY, USA, 2020.

[33] S. Zhang, T. Zheng, Z. Chen, and J. Luo, "Can we obtain fine-grained heartbeat waveform via contact-free rf-sensing?," in *IEEE INFOCOM 2022-IEEE conference on computer communications*, (NA), pp. 1759–1768, IEEE, 2022.

[34] U. M. Khan, L. Rigazio, and M. Shahzad, "Contactless monitoring of ppg using radar," *Proceedings of the ACM on Interactive, Mobile, Wearable and Ubiquitous Technologies*, vol. 6, no. 3, pp. 1–30, 2022.

[35] L. Zhao, R. Lyu, Q. Lin, A. Zhou, H. Zhang, H. Ma, J. Wang, C. Shao, and Y. Tang, "mmarrhythmia: Contactless arrhythmia detection via mmwave sensing," *Proceedings of the ACM on Interactive, Mobile, Wearable and Ubiquitous Technologies*, vol. 8, no. 1, pp. 1–25, 2024.

[36] L. Zhao, R. Lyu, H. Lei, Q. Lin, A. Zhou, H. Ma, J. Wang, X. Meng, C. Shao, Y. Tang, *et al.*, "Airecg: Contactless electrocardiogram for cardiac disease monitoring via mmwave sensing and cross-domain diffusion model," *Proceedings of the ACM on Interactive, Mobile, Wearable and Ubiquitous Technologies*, vol. 8, no. 3, pp. 1–27, 2024.

[37] Y. Yuan, J. Chen, D. Zhang, R. Geng, H. Gong, G. Xu, Y. Pu, Z. Lu, Y. Hu, D. Zhang, *et al.*, "Atrial fibrillation detection via contactless radio monitoring and knowledge transfer," *Nature Communications*, vol. 16, no. 1, p. 4317, 2025.

[38] S. Khare and A. Chawala, "Effect of change in body position on resting electrocardiogram in young healthy adults," *Nigerian Journal of Cardiology*, vol. 13, no. 2, pp. 125–129, 2016.

[39] M. G. Adams and B. J. Drew, "Body position effects on the ecg: implication for ischemia monitoring," *Journal of electrocardiology*, vol. 30, no. 4, pp. 285–291, 1997.

[40] A. Singh, S. U. Rehman, S. Yongchareon, and P. H. J. Chong, "Modelling of chest wall motion for cardiorespiratory activity for radar-based ncvs systems," *Sensors*, vol. 20, no. 18, p. 5094, 2020.

[41] M. Pänkäälä, T. Koivisto, O. Lahdenoja, T. Kiviniemi, A. Saraste, T. Vasankari, and J. Airaksinen, "Detection of atrial fibrillation with seismocardiography," in *2016 38th Annual International Conference of the IEEE Engineering in Medicine and Biology Society (EMBC)*, pp. 4369–4374, IEEE, 2016.

[42] Wikipedia contributors, "Cross-correlation," 2025. Accessed: 2025-09-21.

[43] T. Instruments, "Awr1642boost," 2024. Accessed: 2024-10-29.

[44] P. Senin, "Dynamic time warping algorithm review," *Information and Computer Science Department University of Hawaii at Manoa Honolulu, USA*, vol. 855, no. 1-23, p. 40, 2008.

[45] N. Support, "Mdape - median absolute percentage error," -. Accessed April 3, 2025.

[46] E. R. Pfeiffer, J. R. Tangney, J. H. Omens, and A. D. McCulloch, "Biomechanics of cardiac electromechanical coupling and mechanoelectric feedback," *Journal of biomechanical engineering*, vol. 136, no. 2, p. 021007, 2014.

[47] R. Ripa, T. George, K. R. Shumway, and Y. Sattar, "Physiology, cardiac muscle," in *StatPearls [Internet]*, StatPearls Publishing, 2023.

[48] Cleveland Clinic, "Heart Chambers," 2022. Accessed: 2025-06-13.

[49] A. W. Bowman and S. J. Kovacs, "Assessment and consequences of the constant-volume attribute of the four-chambered heart," *American Journal of Physiology-Heart and Circulatory Physiology*, vol. 285, no. 5, pp. H2027–H2033, 2003.

[50] H. Maeda, "Quantification of synchronous contraction of left ventricle in normal subjects using ecg-gated-spect images," *Physiological measurement*, vol. 25, no. 1, p. 71, 2003.

[51] National Heart, Lung, and Blood Institute, "The Heart: An Owner's Guide," 2024. Accessed: 2025-06-13.

[52] S. Prabhu, A. J. McLellan, T. E. Walters, M. Sharma, A. Voskoboinik, and P. M. Kistler, "Atrial structure and function and its implications for current and emerging treatments for atrial fibrillation," *Progress in cardiovascular diseases*, vol. 58, no. 2, pp. 152–167, 2015.

[53] J. P. Pirruccello, P. Di Achille, S. H. Choi, J. T. Rämö, S. Khurshid, M. Nekoui, S. J. Jurgens, V. Nauffal, S. Kany, FinnGen, *et al.*, "Deep learning of left atrial structure and function provides link to atrial fibrillation risk," *Nature Communications*, vol. 15, no. 1, p. 4304, 2024.

[54] L. Li, V. A. Zimmer, J. A. Schnabel, and X. Zhuang, "Medical image analysis on left atrial lge mri for atrial fibrillation studies: A review," *Medical image analysis*, vol. 77, p. 102360, 2022.

[55] L. Di Biase, P. Santangeli, M. Anselmino, P. Mohanty, I. Salvetti, S. Gili, R. Horton, J. E. Sanchez, R. Bai, S. Mohanty, *et al.*, "Does the left atrial appendage morphology correlate with the risk of stroke in patients with atrial fibrillation? results from a multicenter study," *Journal of the American College of Cardiology*, vol. 60, no. 6, pp. 531–538, 2012.

[56] R. Beinart, S. Abbara, A. Blum, M. Ferencik, K. Heist, J. Ruskin, and M. Mansour, "Left atrial wall thickness variability measured by ct scans in patients undergoing pulmonary vein isolation," *Journal of cardiovascular electrophysiology*, vol. 22, no. 11, pp. 1232–1236, 2011.

[57] Q. Zhang, J.-f. Wang, Q.-q. Dong, Q. Yan, X.-h. Luo, X.-y. Wu, J. Liu, and Y.-p. Sun, "Evaluation of left atrial volume and function using single-beat real-time three-dimensional echocardiography in atrial fibrillation patients," *BMC medical imaging*, vol. 17, pp. 1–6, 2017.

[58] T. Zheng, Z. Chen, S. Ding, and J. Luo, "Enhancing rf sensing with deep learning: A layered approach," *IEEE Communications Magazine*, vol. 59, no. 2, pp. 70–76, 2021.

[59] S. Assana, *Cardiovascular activity monitoring using mmWaves*. PhD thesis, Massachusetts Institute of Technology, 2020.

[60] P. Holoborodko, "Smooth low-noise differentiators," 2024. Accessed: 2024-10-18.

[61] P. Velickovic, G. Cucurull, A. Casanova, A. Romero, P. Lio, Y. Bengio, *et al.*, "Graph attention networks," *stat*, vol. 1050, no. 20, pp. 10–48550, 2017.

[62] K. He, X. Zhang, S. Ren, and J. Sun, "Deep residual learning for image recognition," in *2016 IEEE Conference on Computer Vision and Pattern Recognition (CVPR)*, vol. NA, (Las Vegas, NV, USA), pp. 770–778, IEEE, 2016.

[63] P. Veličković, G. Cucurull, A. Casanova, A. Romero, P. Liò, and Y. Bengio, "Graph attention networks," 2018.

[64] H.-Y. Chang, C.-H. Hsu, and W.-H. Chung, "Fast acquisition and accurate vital sign estimation with deep learning-aided weighted scheme using fmcw radar," in *2022 IEEE 95th Vehicular Technology Conference: (VTC2022-Spring)*, (Helsinki, Finland), pp. 1–6, IEEE, 2022.

[65] L. Xu, J. Lien, H. Li, N. Gillian, R. Nongpiur, J. Li, Q. Zhang, J. Cui, D. Jorgensen, A. Bernstein, L. Bedal, E. Hayashi, J. Yamanaka, A. Lee, J. Wang, D. Shin, I. Poupyrev, T. Thormundsson, A. Pathak, and S. Patel, "Soli-enabled noncontact heart rate detection for sleep and meditation tracking," *Scientific Reports*, vol. 13, no. 1, p. 18008, 2023.

[66] T. Schlagenhauf, J. Wolf, and A. Puchta, "Convolutional-based encoder–decoder network for time series anomaly detection during the milling of 16mncr5," *Data*, vol. 7, no. 12, p. 175, 2022.

[67] E. Fotiadou, T. Konopczyński, J. Hesser, and R. Vullings, "End-to-end trained encoder–decoder convolutional neural network for fetal electrocardiogram signal denoising," *Physiological measurement*, vol. 41, no. 1, p. 015005, 2020.

[68] R. Llugsi, S. El Yacoubi, A. Fontaine, and P. Lupera, "A novel encoder-decoder structure for time series analysis based on bayesian uncertainty reduction," in *2021 IEEE Latin American Conference on Computational Intelligence (LA-CCI)*, (Temuco, Chile), pp. 1–6, IEEE, 2021.

[69] A. Graves and J. Schmidhuber, "Framewise phoneme classification with bidirectional lstm networks," in *Proceedings. 2005 IEEE International Joint Conference on Neural Networks, 2005.*, vol. 4, (Montreal, QC, Canada), pp. 2047–2052 vol. 4, IEEE, 2005.

[70] S. Hochreiter and J. Schmidhuber, "Long Short-Term Memory," *Neural Computation*, vol. 9, pp. 1735–1780, 11 1997.

[71] D. Makowski, V.-Q. Pham, Z. J. Lau, J. C. Brammer, P. Lespinasse, H. Pham, J. Lim, D. Xiao, S. K. Chen, J. T. Wixted, *et al.*, "Neurokit2: A python toolbox for neurophysiological signal processing," *Behavior Research Methods*, vol. -, no. -, pp. 1–16, 2020.

[72] H. V. Huikuri and P. K. Stein, "Heart rate variability in risk stratification of cardiac patients," *Progress in cardiovascular diseases*, vol. 56, no. 2, pp. 153–159, 2013.

[73] C. Ma, H. Xu, M. Yan, J. Huang, W. Yan, K. Lan, J. Wang, and Z. Zhang, "Longitudinal changes and recovery in heart rate variability of young healthy subjects when exposure to a hypobaric hypoxic environment," *Frontiers in Physiology*, vol. 12, p. 688921, 2022.

[74] D. Makowski, T. Pham, Z. J. Lau, J. C. Brammer, F. Lespinasse, H. Pham, and C. Schölzel, "Neurokit2: Heart rate variability (hrv)," 2021. Accessed: 2025-05-11.

[75] F. Shaffer and J. P. Ginsberg, "An overview of heart rate variability metrics and norms," *Frontiers in public health*, vol. 5, p. 258, 2017.

[76] L. Breiman, "Random forests," *Machine learning*, vol. 45, pp. 5–32, 2001.

[77] P. Yang, D. Wang, W.-B. Zhao, L.-H. Fu, J.-L. Du, and H. Su, "Ensemble of kernel extreme learning machine based random forest classifiers for automatic heartbeat classification," *Biomedical Signal Processing and Control*, vol. 63, p. 102138, 2021.

[78] T. Instruments, "Dca1000evm data capture card user's guide," *Heart rhythm*, vol. NA, no. NA, pp. 1–28, 2024. Accessed: 2024-10-29.

[79] T. Instruments, "Mmwave-studio," 2024. Accessed: 2024-10-29.

[80] S. Sensing, "Shimmer 3 ecg unit," 2024. Accessed: 2024-10-28.

[81] M. Abadi, A. Agarwal, P. Barham, E. Brevdo, Z. Chen, C. Citro, G. S. Corrado, A. Davis, J. Dean, M. Devin, S. Ghemawat, I. Goodfellow, A. Harp, G. Irving, M. Isard, Y. Jia, R. Jozefowicz, L. Kaiser, M. Kudlur, J. Levenberg, D. Mané, R. Monga, S. Moore, D. Murray, C. Olah, M. Schuster, J. Shlens, B. Steiner, I. Sutskever, K. Talwar, P. Tucker, V. Vanhoucke, V. Vasudevan, F. Viégas, O. Vinyals, P. Warden, M. Wattenberg, M. Wicke, Y. Yu, and X. Zheng, "TensorFlow: Large-scale machine learning on heterogeneous systems," 2015. Software available from tensorflow.org.

[82] NVIDIA Corporation, "NVIDIA GeForce RTX 20 Series Graphics Cards," 2025. Accessed: 2025-05-25.

[83] J. D. Novaković, A. Veljović, S. S. Ilić, Ž. Papić, and M. Tomović, "Evaluation of classification models in machine learning," *Theory and Applications of Mathematics & Computer Science*, vol. 7, no. 1, p. 39, 2017.

[84] Mayo Clinic, "Electrocardiogram (ecg or ekg)," 2024. Accessed: 2025-05-02.

[85] S. Preejith, R. Dhinesh, J. Joseph, and M. Sivaprakasam, "Wearable ecg platform for continuous cardiac monitoring," in *2016 38th Annual International Conference of the IEEE Engineering in Medicine and Biology Society (EMBC)*, pp. 623–626, IEEE, 2016.

[86] U. Ha, S. Madani, and F. Adib, "Wistress: Contactless stress monitoring using wireless signals," *Proceedings of the ACM on Interactive, Mobile, Wearable and Ubiquitous Technologies*, vol. 5, no. 3, pp. 1–37, 2021.